Arch. Metall. Mater. **63** (2018), 3, 1077-1082

DOI: 10.24425/123778

A. ZIĘBOWICZ*#, A. WOŹNIAK**, B. ZIĘBOWICZ**, K. KOSIEL***, G. CHLADEK**

THE EFFECT OF ATOMIC LAYER DEPOSITION OF ZrO_2 ON THE PHYSICOCHEMICAL PROPERTIES OF COBALT BASED ALLOYS INTENDED FOR PROSTHETIC DENTISTRY

The paper presents the effect of ZrO_2 layer deposition by the ALD process on the physicochemical properties of cobalt-based alloys (Realloy C and EOS CoCr SP2) intended for application in prosthetic dentistry. The paper shows the results of the surface roughness measurements made by the AFM method as well as the wettability and free surface energy measurements. Additionally, potentiodynamic tests of pitting corrosion resistance and electrochemical impedance spectroscopy in a solution of artificial saliva were carried out. Tests were carried out on the samples in the initial state and after surface modification with the ZrO_2 layer. Based on these results, the usefulness (e.g. enhancement of corrosion resistance and biocompatibility) of the proposed ZrO_2 layer on the cobalt alloys was assessed.

Keywords: Cobalt alloy; ZrO_2 layer; SFE; Corrosion; Artificial saliva

1. Introduction

The dental materials used for manufacturing prosthetic restorations must be characterized by biocompatibility and corrosion resistance in the oral environmental. However, corrosion products and metal ions could be released from the alloy and could cause an allergic reaction in a sensitized patient. The relationship between pre-existing metal sensitivity and implant-related (prosthetic device) contact dermatitis or implant failure remains unclear and therefore nearly impossible to predict. The human stomatognathic system is subjected to varying changes in temperature and pH, which is why this dynamic microenvironment allows for unpredictable conditions that may actually enable biocorrosion. In dental applications the most popular metal biomaterials are cobalt-based alloys. Due to the constantly rising performance requirements, materials used for manufacturing prosthetic restorations must be characterized by biocompatibility, good corrosion resistance and satisfying mechanical properties. All of the properties of a material are inherently related with its chemical composition and structure. Meanwhile the structure of a material is dependent on the type of manufacturing technology [1-8]. Currently, modern CAD/CAM systems based on 3D printing are increasingly used in dental applications and thus they become alternatives to the traditional method of casting. The Direct Metal Laser Sintering (DMLS) procedure is among the most popular 3D methods. The elements produced with the use of the DMLS method are characterized by i.e. high dimensional accuracy [9-14].

It should generally be emphasized, that the oral environment is an extremely aggressive corrosive environment. That is why, the current research on biomaterials used in the stomatognathic system, includes the modification of its surface as a strategy to improve the biocompatibility or to enhance the functionality of the biomaterial in an environment of saliva. In order to prevent degradation of dental materials, their surface can be modifiedby a thin oxide layer. One promising method seems to be the atomic layer deposition (ALD) method. The oral environment and the effect of tribological wear of prosthetic restorations could cause a faster degradation process. In view of this fact, the ALD method has been used more and more often. ALD is characterized by sequencing of the process and the self-limitation of layer growth. The sequencing character of the process is based on the fact that the precursors are alternately introduced to the chamber. In the next step the chamber is washed by inert gas. Based on this the ALD process offers high quality, chemical homogeneity and control (at the Angstrom level) the thickness of the deposited layer [14-21].

2. Materials and methods

The subject of the study was cobalt – based alloys, divided into two groups by the manufacturing technology. The first group of samples was obtained by traditional casting techniques (Realloy C), and the second by Direct Metal Laser Sintering (EOS

* SILESIAN UNIVERSITY OF TECHNOLOGY, DEPARTMENT OF BIOMATERIALS AND MEDICAL DEVICES ENGINEERING, ZABRZE, POLAND
** SILESIAN UNIVERSITY OF TECHNOLOGY, GLIWICE, DEPARTMENT OF BIOMEDICAL MATERIALS ENGINEERING, POLAND
*** INSTITUTE OF ELECTRON TECHNOLOGY, DEPARTMENT OF MICRO- AND NANOTECHNOLOGY OF WIDE BANDGAP SEMICONDUCTORS, WARSAW, POLAND
# Corresponding author: anna.ziebowicz@polsl.pl

CoCr SP2). The chemical composition of the tested alloys is shown in Table 1. The samples were subjected to mechanical treatment: mechanical grinding with the use SiC abrasive paper with grain sizes of 320, 500, 800 and 1000 and mechanical polishing, performed with SiO_2 polishing paste. The mechanical treatment was carried out with the use of polishing – grinding machine Tergamin –30 by Struers.

TABLE 1

Chemical composition of tested alloys

Material		Elements, [%]						
	Co	Cr	Mo	W	N	Si	Fe	Mn
Realloy C	59.00	25.00	3.90	10.10	0.19	1.60	—	0.75
EOS CoCr SP2	63.80	24.70	51.00	5.40	—	1.00	>0.50	>1.00

The surface modification of the tested samples was performed at the Institute of Electron Technology in Warsaw. A zirconia oxide layer was deposited by the ALD method in a TFS – 200 – 190 reactor by Beneq. During the ALD process, the 6N-purity argon pressure inside the reactor was approximately 2 mbar. TEMAZr was used as a precursor for zirconia and deionized water for the oxide and argon as an inert gas. Growth per cycle (GPC) for ZrO_2 (at the ALD process temperature of 200°C) was approximately 0.092 nm/cycle.

2.1. Atomic force microscopy

In order to determine the surface topography, atomic force microscopy was performed. For this purpose, an XE-100 microscope by Park Systems with a non-contact mode was used. The obtained results were determined by parameters describing the surface roughness: the Root Mean Square, (RMS/R_q), the arithmetic average of ordinates profile (R_a) and sum of the maximum height and maximum depth (ΔZ). The parameters were calculated over three scan areas of 25 × 25 μm, 10 × 10 μm and 2 × 2 μm.

2.2. Wettability and free surface energy tests

The contact angle measurements were performed in order to determine the physicochemical properties. The study was carried out with the use of a test stand, incorporating a Surftronic Universal goniometer by OGE and a PC with Surface 4.5 software to analyse to recorded drop image. Drops of the measured liquids (distilled water and diiodomethane), each 1.5 μl in volume, were placed on the surface of the tested samples. The measurements were performed at a room temperature $T = 23$°C and started 20 s after dispensing the drops on the samples. The values of surface free energy (SFE) and their polar and dispersion properties for the Owens-Wendt method are given in Table 2.

TABLE 2

The values of SFE and their polar and apolar components for liquids used in Owens – Wendt method

Measure liquid	γ_L, [mJ/m^2]	γ_L^d, [mJ/m^2]	γ_L^P, [mJ/m^2]
Distilled water	72.80	21.80	51.00
Diiodomethane	50.80	50.80	0.00

2.3. Electrochemical impedance spectroscopy

In order to obtain information on the physiochemical properties, electrochemical impedance spectroscopy was conducted. The test stand included an AutoLab PGSTAT 302N system with an FRA2 module (Frequency Response Analyzer) and three-electrode system, where the working electrode was represented by the test sample, the auxiliary electrode was a platinum wire (PTP-201) and the reference electrode was in the form of a calomel electrode (SEC KP-113). The research was carried out in the frequency range of 10^4-10^{-3} Hz. The amplitude of the sinusoidal signal that actuated the tension amounted to 10 mV. The impedance system spectra in the form of Bode`s diagrams and in the form of Nyquit diagrams for different values of frequency were determined. The obtained measurement data were adjusted to the substitute setup. On this basis, the numerical values of resistance R and capacity C of analysed systems were determined. The EIS test was carried out in artificial saliva (pH = 6.5-6.8) at temperature $T = 37 \pm 1$°C. The chemical composition of the artificial saliva solution was in line with recommendations of the ISO standard [22].

2.4. Potentiodynamic polarization

In order to determine the resistance to pitting corrosion, potentiodynamic tests were carried out by recording anodic polarization curves as recommended by the ISO 10993-15 standard [23]. The measurement was performed with the use a VoltaLab PGP201 potentiostat, a computer with VoltaMaster 4 software and an electrochemical cell with a three-electrode system (identical to that used in the corrosion test). In the first step, the open circuit potential E_{ocp} was determined. Next the anodic polarization curves were recorded from the initial potential $E_{int} = E_{ocp} - 100$ mV. The polarization rate was equal to 3 m/s and the potential change was in the direction of the anode. Once the anodic current density reached $i = 1$ mA/cm^2, the polarization direction was changed and the return curves were recorded. On this basis, the characteristic parameters of corrosion were set: corrosion potential E_{corr} [mV], breakdown potential E_{np} [mV], repassivation potential E_{cp} [mV], and transpassivation potential E_{tr} [mV]. The value of polarization resistance R_p [kΩ·cm^2] was determined by the Stern method. The pitting corrosion test was carried out in identical conditions to the EIS test.

3. Results and discussion

3.1. Atomic force microscopy

The results of AFM observation for both material are presented in Figs. 1, and 2. The characteristic values describing the surface roughness are shown in Table 3. The highest values of surface roughness were obtained for the cast samples in the initial state. The mean values of parameters in the output state of scan areas were as follows: for the 25 × 25 scan area, $\Delta Z_{max} = 1915$ nm, $R_q = 97$ nm and $R_a = 84$ nm; for the 10 × 10 µm scan area, $\Delta Z_{max} = 1358$ nm, $R_q = 78$ nm and $R_a = 67$ nm; and for the 2 × 2 µm scan area, $Z_{max} = 316$ nm, $R_q = 26$ nm, and $R_a = 19$ nm. For the EOS CoCr SP2 samples in the initial state recorded the lowest values and the mean values were as follows: for the 25 × 25 µm scan area, $\Delta Z_{max} = 265$ nm, $R_q = 83$ nm, and $R_a = 67$ nm; for the 10 × 10 µm scan area, $\Delta Z_{max} = 273$ nm, $R_q = 39$ nm, and $R_a = 32$ nm; and for the 2 × 2 µm scan area, $Z_{max} = 89$ nm, $R_q = 19$ nm, and $R_a = 17$ nm. With deposited ZrO_2 layer the surface roughness parameter for the cast samples decreased and the mean values were as follows: for the 25 × 25 µm scan area, $\Delta Z_{max} = 377$ nm, $R_q = 98$ nm, and $R_a = 84$ nm; for the 10 × 10 µm scan area, $\Delta Z_{max} = 348$ nm, $R_q = 60$ nm, and $R_a = 52$ nm; and for the 2 × 2 µm scan area, $\Delta Z_{max} = -101$ nm, $R_q = 22$ nm, and $R_a = 19$ nm. For the samples obtained from the DMLS method with the ZrO_2 layer, the values of surface roughness parameters were similar to the values of samples in initial state. Based on the obtained results, it can be concluded that for the all analyzed samples, the values of the roughness parameter for the smallest scan areas decreased.

TABLE 3

The results of surface roughness by the AFM method

Area, [µm × µm]	25 × 25			10 × 10			5 × 5		
	ΔZ_{max}	R_q	R_a	ΔZ_{max}	R_q	R_a	ΔZ_{max}	R_q	R_a
Realloy C_is	1915	97	84	1358	78	67	316	26	19
EOS CoCr SP2_is	265	83	67	273	39	32	89	19	17
Realloy C_ald	337	98	84	348	60	52	–101	22	19
EOS CoCr SP2_ald	333	70	59	270	67	51	95	34	25

3.2. Wettability and free surface energy tests

The obtained results of the contact angle and SFE calculation are presented in TABLE 4. The average value of the contact angle of cast samples in the initial state was 82.75°. The contact angle values of less than 90° indicate the hydrophilic character of the surface. Meanwhile, the mean value of the contact angle of the samples obtained from the DMLS procedure was 91.83° and pointed to the hydrophobic character of the surface. It was observed that the wettability, similarly to the surface roughness value, decreased due to the deposition of the ZrO_2 layer on the surface of both material variants. For the cast samples with ZrO_2 layer, the mean value of contact angle was 114.06° and for the EOS samples it was 105.69°. The values of surface free energy γ were comparable for all tested samples. The obtained high value of the apolar component and the low values of the polar components allowed it to be concluded that the surface of

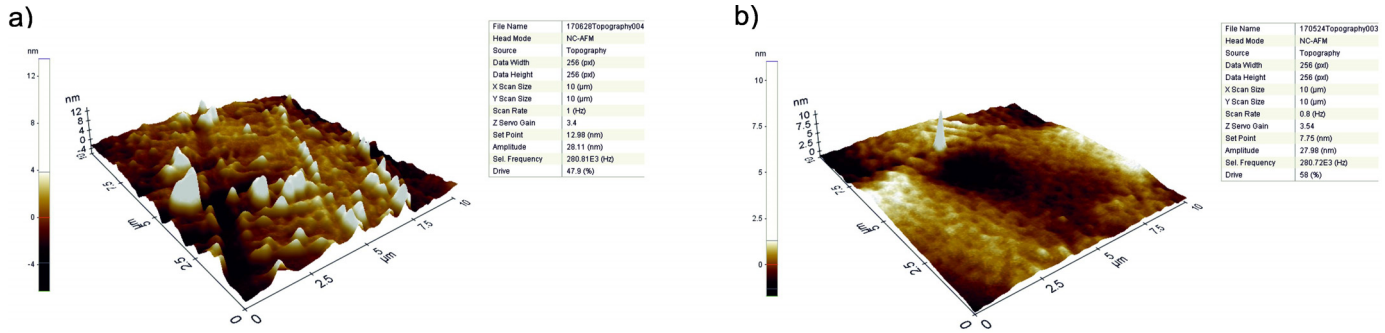

Fig. 1. Surface geometry of the Realloy C: a) initial state, b) with ZrO_2 layer

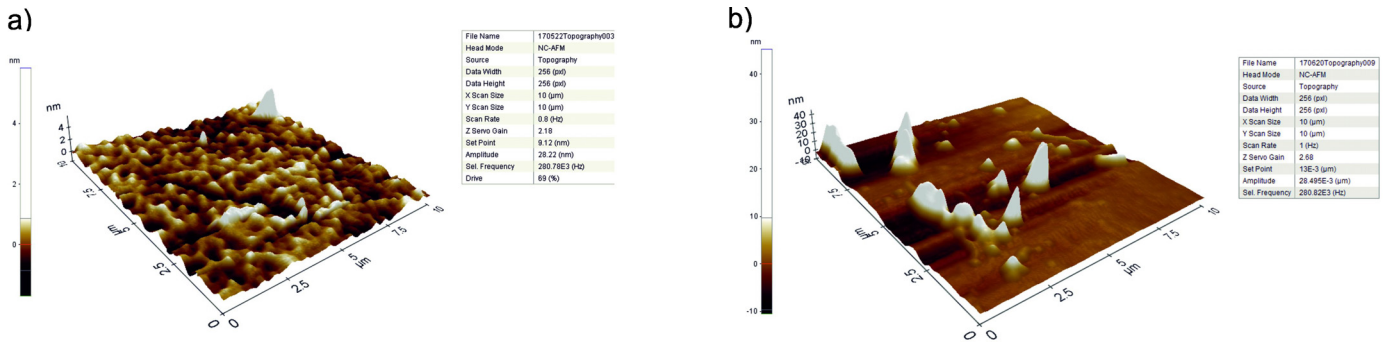

Fig. 2. Surface geometry of the EOS CoCr SP2: a) initial state, b) with ZrO_2 layer

tested samples exhibited a greater affinity for the apolar groups than to the polar ones.

TABLE 4

The results of wettability and surface free energy

Sample	Contact angle, [°]		Surface free energy, [mJ/m^2]		
	Distilled water	Diiodo-methane	γ_s	γ_L^d	γ_L^P
Realloy C_is	82.75	54.24	32.82	27.83	6.59
EOS CoCr SP2_is	91.83	57.31	30.58	28.43	2.15
Realloy C_ald	114.06	54.02	47.38	44.83	2.56
EOS CoCr SP2_ald	105.69	54.63	38.89	38.00	0.89

3.3. Electrochemical impedance spectroscopy

The obtained results of the electrochemical impedance spectroscopy test in the form of impedance spectra are shown in Figs. 3 and 4. On the basis of the recorded spectra the electric values were determined, and are presented in Table 5. The best fit of the model spectra to the impedance spectra for both variants of material in the initial state and with the ZrO_2 layer was provided by the equivalent circuit composed of two parallel electric elements representing capacitive or constants of border combined with resistance transitions and resistance (Fig. 5). In the figures, R_{ct} denotes the resistance of the charge transfer, CPE_{dl} the capacity of the oxide layer, R_{pore} the resistance of electrolyte in the porous phase, C_{pore} the capacity of double layer, and R_s the resistance of the artificial saliva solution. That indicates the presence of a double layer with different values of charge transfer resistance R_{ct}. The values were equal to $R_{ct} = 4.93$ MΩcm^2 for Realloy C_is, $R_{ct} = 3.85$ MΩcm^2 for EOS CoCr SP2_is, $R_{ct} = 23.11$ MΩcm^2 for Realloy C with ZrO_2 and $R_{ct} = 30.00$ MΩcm^2 for EOS CoCr SP2 after the ALD process. The set of Nyquist diagrams for all the tested samples presented of fragments of incomplete semicircles. This was a typical impedance response for an oxide thin layer. The maximum values of phase displacement at a broad range of frequencies of the samples in the initial state for both materials were similar and amounted to $\theta = 80$-70°. Meanwhile, for the samples with ZrO_2

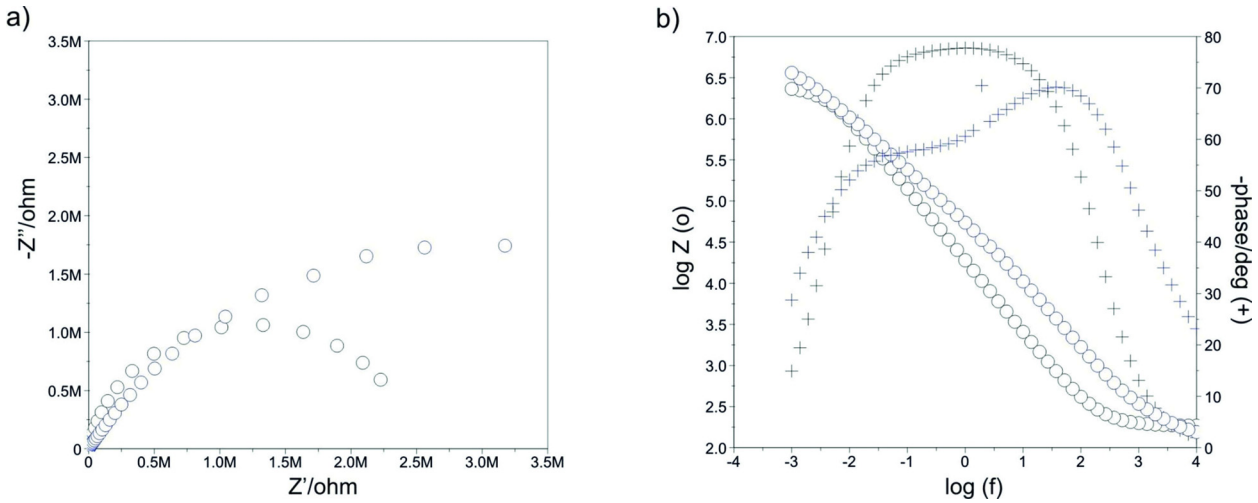

Fig. 3. Sample spectra impedance for the Realloy C samples in initial state and with ZrO2 layer: a) Nyquist diagram, b) Bode`s diagram

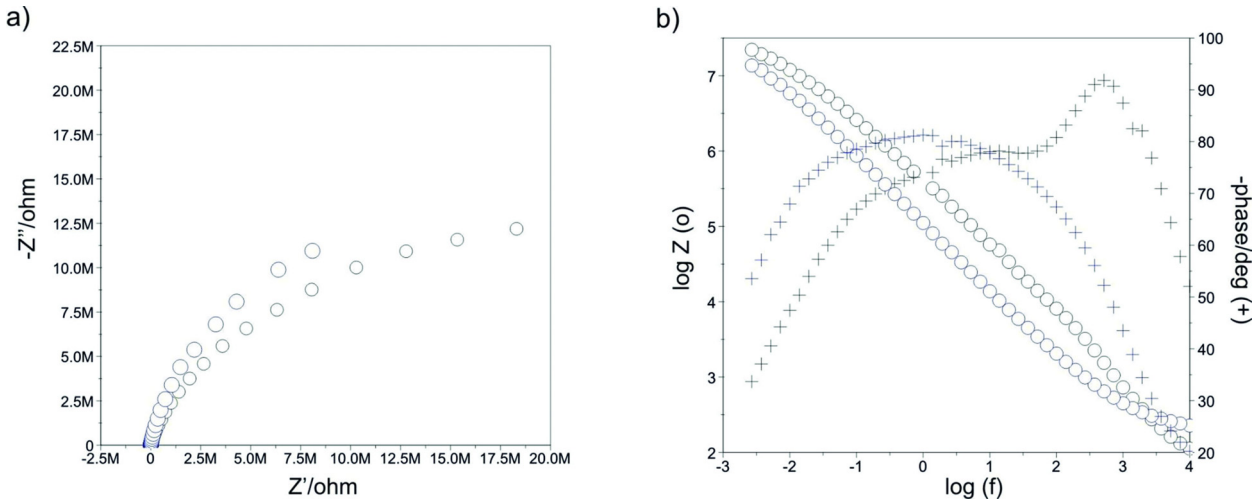

Fig. 4. Sample spectra impedance for the EOS CoCr SP2 samples in initial state and with ZrO2 layer: a) Nyquist diagram, b) Bode's diagram

TABLE 5

The results of the electrochemical impedance spectroscopy

Sample	E_{ocp}, [mV]	R_s, [kΩcm^2]	R_{pore}, [kΩcm^2]	CPE_{pore}		R_{st}, [MΩcm^2]	CPE_{dl}	
				Y, [Ω^{-1} cm^{-n}s^{-n}]	n		Y, [Ω^{-1} cm^{-n}s^{-n}]	n
Realloy C_is	–257	55	40.10	0.8553E-5	0.87	4.93	0.6732E-5	0.74
EOS CoCr SP2_is	–331	55	0,188	0.1055E-4	0.93	3.85	0.4567E-3	0.60
Realloy C_ald	–250	55	613	0.7440E-6	0.95	23.11	0.7616E-6	0.92
EOS CoCr SP2_ald	–131	55	0,449	0.9498E-4	0.63	30.00	0.1844E-5	0.88

layer, the maximum value of phase displacement in the case of Realloy C material was $\theta = 75°$ and that for the EOS CoCr SP2 material was $\theta = 65°$. The inclinations $\log|Z|$ in the whole scope of the frequency change were close to –1.

$$Z = R_s + \frac{1}{\frac{1}{R_{pore}} + Y_{pore}(j\omega)^{n_{pore}}} + \frac{1}{\frac{1}{R_{Ct}} + Y_0(j\omega)^{n_0}}$$

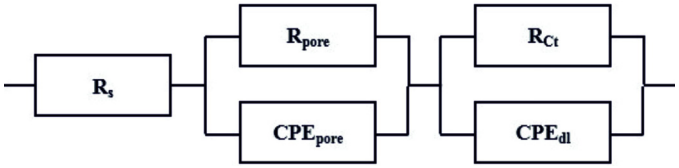

Fig. 5. Equivalent electric substitute circuit

3.4. Potentiodynamic polarization

The obtained results of the pitting corrosion test for samples in initial the state are presented in Fig. 6, while the polarization curves for the samples with the ZrO_2 layer are presented in Fig. 7. The characteristic values describing the pitting corrosion are shown in Table 6. For both tested alloys in the initial state, the polarization curves had a similar character and no hysteresis loops were stated. It was determined the value of the transpassivation potential and the mean value for cast sample was E_{tr} = 837 mV and that for EOS CoCr SP2_is was E_{tr} = 875 mV. For the cast samples after surface modification, similarly to the samples in the initial state, the progress of the polarization curves was characteristic for materials with high corrosion resistance. The mean value of transpassivation potential for Realloy C_ald samples was E_{tr} = 1324 mV and was higher compared to the samples in the initial state. In case of the EOS CoCr SP2 samples with the deposited ZrO_2 layer, the existence of breakdown potential E_b = 1320 mV and repassivation potential E_{cp} = 793 mV has been stated. However the mean value of breakdown potential was higher compared to the transpassivation potential for samples in the initial state. On the basis of the obtained results, it was found that the deposition of the ZrO_2 layer on the surface of both material was beneficial for the corrosion resistance.

TABLE 6

The results of the potentiodynamic tests

Sample	E_{corr}, [mV]	E_{tr}, [mV]	E_b, [mV]	E_{cp}, [mV]	R_p, [kΩ/cm^2]
Realloy C_is	–182	837	—	—	15
EOS CoCr SP2_is	–273	875	—	—	490
Realloy C_ald	–173	1324	—	—	21
EOS CoCr SP2_ald	–208	—	1320	793	126

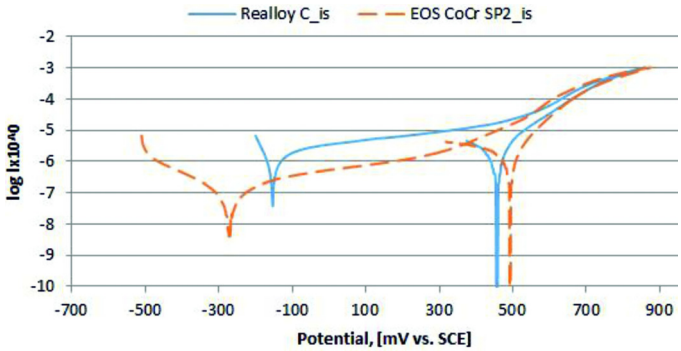

Fig. 6. Example of polarization curves for materials in initial state

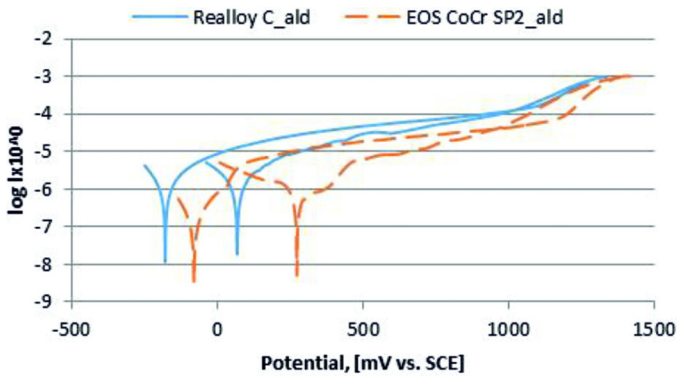

Fig. 7. Example of polarization curves for materials with ZrO2 layer

4. Conclusion

Correct selection of the physical and chemical properties is a significant issue in the process of adjusting the functionalities of, for example crowns or bridges, and has a direct impact on the final quality of the prosthetic devices. One of many physicochemical properties, that decide the quality of the prosthetic material, is its wettability, which is related to physical phenomena occurring on its surface. These phenomena are mainly connected with the surface energy, whose value determines the speed and

degree of factors such as plaque aggregation, water absorbability, hydrophilicity, or hydrophobicity of a given material.

Based on the results obtained it can be concluded that the physicochemical properties of cobalt-based alloy differed depending on the type of manufacturing technology. For alloys used in dental applications, the hydrophobic character of the surface and low values of the R_a parameters are more favorable. The samples obtained from DMLS technology were characterized by lower values of roughness and contact angle. The tested alloys were characterized by similar corrosion resistance: the transpassivation potential has been stated. Additionally, it can be concluded that the thin ZrO_2 layer deposited on the surfaces of both materials affects the improvement of their utility properties. For the cast samples with deposition on their surface oxide layer the values of the roughness parameters R_a decreased. In the case of the samples obtained by 3D printing, the ZrO_2 layer reconstructed the topography of the samples in the initial state. Additionally, for both variants of material, the surface modification affects the reduction of the wettability and increases the pitting corrosion resistance. The breakdown potential obtained for the DMLS samples with the ZrO_2 layer was higher compared to the value of the transpassivation potential for samples in the initial state.

REFERENCES

[1] J. Augustyn-Pieniążek, A. Łukaszczyk, J. Loch, Eng. Biomater. **18** (130), 2-9 (2015).

[2] J. Augustyn-Pieniążek, P. Kurtyka, J. Stopka, Eng. Biomater. **17** (127), 7-15 (2014).

[3] M. Walczak, K. Beer, B. Surowska, J. Borowicz, Arch. Civ. Mech. Eng. **12** (2), 171-177 (2012).

[4] M. Podrez-Radziszewska, K. Haimann, W. Dudziński, M. Morawska-Sołtysik, Arch. Foundry Eng. **10** (3), 51-56 (2010).

[5] ISO 22674:2016 Preview Dentistry – Metallic materials for fixed and removable restorations and appliances.

[6] E. Sobolewska, Annales Academiae Medicae Stetinensis **56** (3), 66-80 (2010).

[7] Ł. Bojko, A.M. Ryniewicz, R. Bogucki, P. Pałka, Prz. Elektrotech. **91** (5), 29-32 (2015).

[8] J.K. Pietruski, M.D. Pietruska, Stomatol. Estet. **9** (3), 89-99 (2013).

[9] S. Majewski, Prot. Stoma. **57** (1), 124-131 (2007).

[10] K. Vijay Venekastesh, V. Widyashree Nadini, J. Indian Prosthodont Soc. **14** (4), 389-392 (2013).

[11] D. Nakonieczny, A. Ziębowicz, Z. Paszenda, C. Krawczyk, Biocybern. Biomed. Eng. **37** (1), 229-245 (2017).

[12] A. Ziębowicz, B. Bączkowski, Numerical analysis of the implant – abutment system, in: Piętka, P. Badura, J. Kawa, W. Więcławek (Eds.), Information Technologies in Biomedicine, Springer – Verlag Berlin Heidelberg (2012).

[13] W. Kajzer, A. Kajzer, M. Grygiel-Pradelok, A. Ziębowicz, Evaluation of physicochemical properties of TiO2 layer on AISI 316 LVM steel intended for urology, in: E. Piętka, P. Badura, J. Kawa, W. Więcławek (Eds.), Book Series: Advances in Intelligent Systems and Computing 472, Information Technologies in Biomedicine Springer – Verlag Berlin Heidelberg (2016).

[14] W. Walke, M. Basiaga Z. Paszenda, A. Kajzer, W. Kajzer, J. Szewczenko T. Pustelny, S. Drewniak, Z. Opilski, C. Krawczyk, Surf. Coat. Tech. **307**, 753-760 (2016).

[15] P. Boryło, K. Lukaszkowicz, M. Szindler, M. Basiaga, J. Achiev. Mate.r Manufact. Eng. **73** (2), 86-92 (2015).

[16] Qiuyue Yang, Wei Yuan, Xiangmei Liu, Yufeng Zheng, Zhenduo Cui, Xianjin Yang, Haobo Pan, Shuilin Wu, Acta. Biomat. **58**, 515-526 (2017).

[17] K. Kosiel, M. Dominik, I. Ściślewska, M. Kalisz, M. Guziewicz, K. Gołaszewska, J. Niedziółka-Jonsson, W.J. Bock, M. Śmietana, Nanotech. **29**, 1-13 (2018).

[18] Zehui Liu, Yizhou Zhu, Xiangmei Liu, K.W.K. Yeung, Shuilin Wu, Colloids Surf. Biointerfaces **151**, 165-177 (2017).

[19] Li M., Liu X., Xu Z., Yeung K.W., Wu S., ACS Appl. Mater. Interfaces **8** (49), 33972-33981 (2016).

[20] Xiangmei Liu, Qiuyue Yang, Zhaoyang Li, Wei Yuan, Yufeng Zheng, Zhenduo Cui, Xianjin Yang, Kelvin W.K. Yeung, Shuilin Wu, Appl. Surf. Sci. **434**, 1101-1111 (2018).

[21] https://beneq.com/en/thin-films/technology/atomic-layer-deposition, accessed 04.01.2018

[22] 19ISO 10271:2011 Preview Dentistry – Corrosion test methods for metallic materials.

[23] 20ISO 10993-15:2000 Biological evaluation of medical devices – Part 15: Identification and quantification of degradation products from metals and alloys.